Available online at www.sciencedirect.com
ScienceDirect
Geomorphology 99 (2008) 90–98
GEOMORPHOLOGY
www.elsevier.com/locate/geomorph

Identification of geologic contrasts from landscape dissection pattern: An application to the Cascade Range, Oregon, USA

Wei Luo [a,*], Tomasz Stepinski [b]

[a] Department of Geography, Northern Illinois University, DeKalb, IL 60115, USA
[b] Lunar and Planetary Institute, 3600 Bay Area Boulevard, Houston, TX 77058, USA

Received 29 August 2007; received in revised form 13 October 2007; accepted 15 October 2007
Available online 26 November 2007

Abstract

This paper demonstrates the plausibility of inferring the spatial variability of geology from topographically derived landscape dissection patterns. This enables surveying large regions for spatial variability in geology, for which direct remote sensing is not feasible, by studying variability in dissection pattern, a feature extracted straight off from digital elevation model data. Dissection pattern is obtained automatically by a novel algorithm, especially designed to delineate the valleys with high accuracy in order to reflect spatial variability in dissection density. The dissection pattern is encapsulated by a continuous map of drainage density, a raster variable best suited for showing spatial variability of dissection. Such a map, constructed for the study area in the Cascade Range, Oregon, USA, shows a sharp discontinuity in the dissection pattern, indicating change in underlying geology. Possible factors controlling the dissection pattern such as climate, local and regional slopes, vegetation, and geology are examined, and geology has been found to be the dominant controlling factor. The dissection contrast coincides with the boundary between the Western and High Cascades, two geologic provinces with different rock ages and types. The older and less permeable Western Cascades are associated with denser dissection pattern, whereas the younger and more permeable High Cascades correspond to less dissected pattern. This new mapping method can be applied to locations where topography is the only readily available data, and the generated map could be used to extract previously unknown geologic or environmental information.

Keywords: Landscape dissection; Drainage density; Controlling factors of drainage density; Oregon Cascade Range

1. Introduction

The automated analyses of remotely sensed data have the potential to expedite geologic mapping and exploration. Automated mineral mapping, using multi-spectral images (Van der Meer, 1998), is rather common. However, machine inference of geology from remote sensing eludes robust solution. This is because labeling of geological units requires information that is either difficult to collect remotely or hard to interpret by a computer algorithm. Therefore, most of the existing work (Kruse and Dietz, 1991; Pena and Abdelsalam, 2006) concentrates on acquisition of imagery, radar, and topographic data for a subsequent manual interpretation of geology. These efforts are directed at producing geologic maps of focus areas by combining remotely sensed data with human cognitive abilities. Despite the difficulties, there is an acute interest in automating the process of geology inference by using machine learning techniques utilizing either multi-spectral images (Lucieer et al., 2004), or a fusion of different datasets (Barnett et al., 2004; Bou Kheir et al., 2007). However, most existing methods are limited to small spatial scales and lack robustness. Here we report a novel technique that uses digital elevation model (DEM) data to detect changes in the underlying geology on a regional scale. The idea is to use spatial variability of landscape dissection pattern, which can be extracted from gridded elevation data, to infer spatial distribution of geological units. This fully automated and robust method is not intended to determine the surface extent of specific geologic units, but instead is geared toward finding boundaries between units having contrasting geomorphologic expressions. The landscape dissection pattern is encapsulated by a continuous map of valleys density (Tucker et al., 2001), derived from the distribution of valleys mapped by a computer algorithm from a DEM. In the rest of this paper the

* Corresponding author: Tel.: +1 815 753 6828; fax: +1 815 753 6872.
E-mail address: wluo@niu.edu (W. Luo).

0169-555X/$ - see front matter © 2007 Elsevier B.V. All rights reserved.
doi:10.1016/j.geomorph.2007.10.014

terms stream, valley, and channel are used interchangeably. This should not lead to any confusion as we use these terms only in the context of calculating landscape dissection pattern. The map of drainage density is used to infer boundaries between geologic formations. We applied our technique to a study site in the Cascade Range, Oregon, USA, featuring sharp contrast between the two adjacent geologic provinces. Our automated technique identified contrast in dissection pattern that we were able to link to the geologic contrast, thus validating our methodology. This technique provides automatic means for spotting geologic boundaries on regional scales in places where traditional mapping efforts are hindered by lack of access, and where the geology cannot be interpreted from images.

2. Study area

The study area is located in the Cascade Range, Oregon, between 121.31°W and 122.75°W and between 43.31°N and 45.26°N. The area is roughly 117×216 km (Fig. 1). The DEM of the study area has a spatial resolution of 37.215 m and is available from the National Elevation Dataset (NED, http://seamless.usgs.gov/), a seamless mosaic of best-available elevation data from different sources. Fig. 1 shows a perspective view of the study area and a simplified map of its geology (see Section 3.4 for details). The region encompasses the two major provinces of the Cascade Range in Oregon (Walker and MacLeod, 1991; Sherrod and Smith, 2000): the Western Cascades (the western part of the study area) and the High Cascades (the eastern part). The Western Cascades are dominated by layered, basaltic and andesite lavas, and volcaniclastic flows of Tertiary age, whereas the High Cascades are of Quaternary age and are dominated by low gradient basaltic and andesitic lava flows, cinders, pumice, and volcanic ash (Tague and Grant, 2004). The boundary between these two geologic provinces runs roughly through the middle of the study area from the north to the south (Fig. 1). The two formations have clearly different geomorphologic expression with the High Cascades having higher elevation but lower local relief and lower dissection density, and the Western Cascades having the opposite attributes. These attributes makes the study area an ideal site to test our methodology in revealing underlying geology from spatial dissection pattern derived from topographic data.

3. Methods and results

3.1. Automatic extraction of streams from a DEM

Grid-based digital elevation model (DEM) is a raster that stores topographic elevation of each pixel in a raster node (thereafter referred to as a cell). It is used to calculate flow direction, a staple for determining many important hydrologic parameters. In particular, flow direction is a variable underpinning a number of algorithms for machine delineation of streams from topography that have been implemented in software packages such as ArcGIS, RiverTools and TauDEM (Tarboton and Ames, 2001). We refer to these algorithms collectively as hydrology-based algorithms. A hydrology-based algorithm is determined by two fundamental design choices: how to specify the flow directions, and, given the flow directions, how to separate channels from hillslopes. The simplest method for specifying flow directions is to assign flow from each cell to one of its eight neighbors (O'Callaghan and Mark, 1984; Jenson and Domingue, 1988). This method is referred to as the D8 algorithm for eight flow directions. Flow routing methods avoiding a rough discretization of the D8 algorithm have been also developed (Quinn et al., 1991; Costa-Cabral and Burges, 1994; Tarboton, 1997); however, they produce only subtle differences in the maps of streams on the scale that is of interest here (Tarboton, 1997). Thus, the map of streams, as delineated by a hydrology-based algorithm, depends primarily on the choice of a channelization criterion. Such a criterion uses theoretical or phenomenological insights to prune the raster-filling network of drainage directions into a network of streams. A number of criteria have been proposed, including (1) the contributing area threshold (O'Callaghan and Mark, 1984), (2) the stream order threshold (Peckham, 1995), (3) the contributing area and the slope threshold (Montgomery and Dietrich, 1992), and (4) the contributing area and the stream length threshold (implemented in TauDEM). A contributing area is an area of a drainage basin culminating at a given cell; it is used in channelization thresholds as a proxy for a discharge. It is our assertion that automatic mapping of streams (or valleys) in a landscape characterized by a spatial variability of dissection pattern cannot be achieved satisfactorily by any of hydrology-based algorithms. This is because a threshold in a channelization criterion can be set to reflect only a single dissection pattern.

In order to detect geologic contrast from changing patterns of landscape dissection, we need a method of stream delineation that is capable of handling spatial change. Such a method is offered by a terrain morphology-based method (Molloy and Stepinski, 2007). The morphology-based method does not rely on flow directions and channelization criteria; instead it detects incisions directly from terrain morphology. The basic idea is to map the valleys as parts of the raster having a U-like morphology. Using terrain morphology to extract drainage networks had been proposed in the past (Peuker and Douglas, 1975; Band, 1986; Howard, 1994; Tarboton and Ames, 2001). In particular, Tarboton and Ames (2001) developed a morphology-based delineation method that uses a simple proxy of topographic curvature (Peuker and Douglas, 1975; Band, 1986) to identify channels. Although this method seems to work well for small single basins, it often fails to produce an acceptable map of streams for a large study area like ours. On the other hand, our morphology-based algorithm is especially designed to map large regions characterized by spatially variable dissection. In fact, it has been originally developed and applied to map valley networks or river-like landforms on Mars that lack spatial integration (Luo and Stepinski, 2006). The algorithm calculates the tangential curvature $\kappa_t(x, y)$, a topographic curvature measured in the direction of tangent to contour at a given point (x, y) (Mitasova and Hofierka,

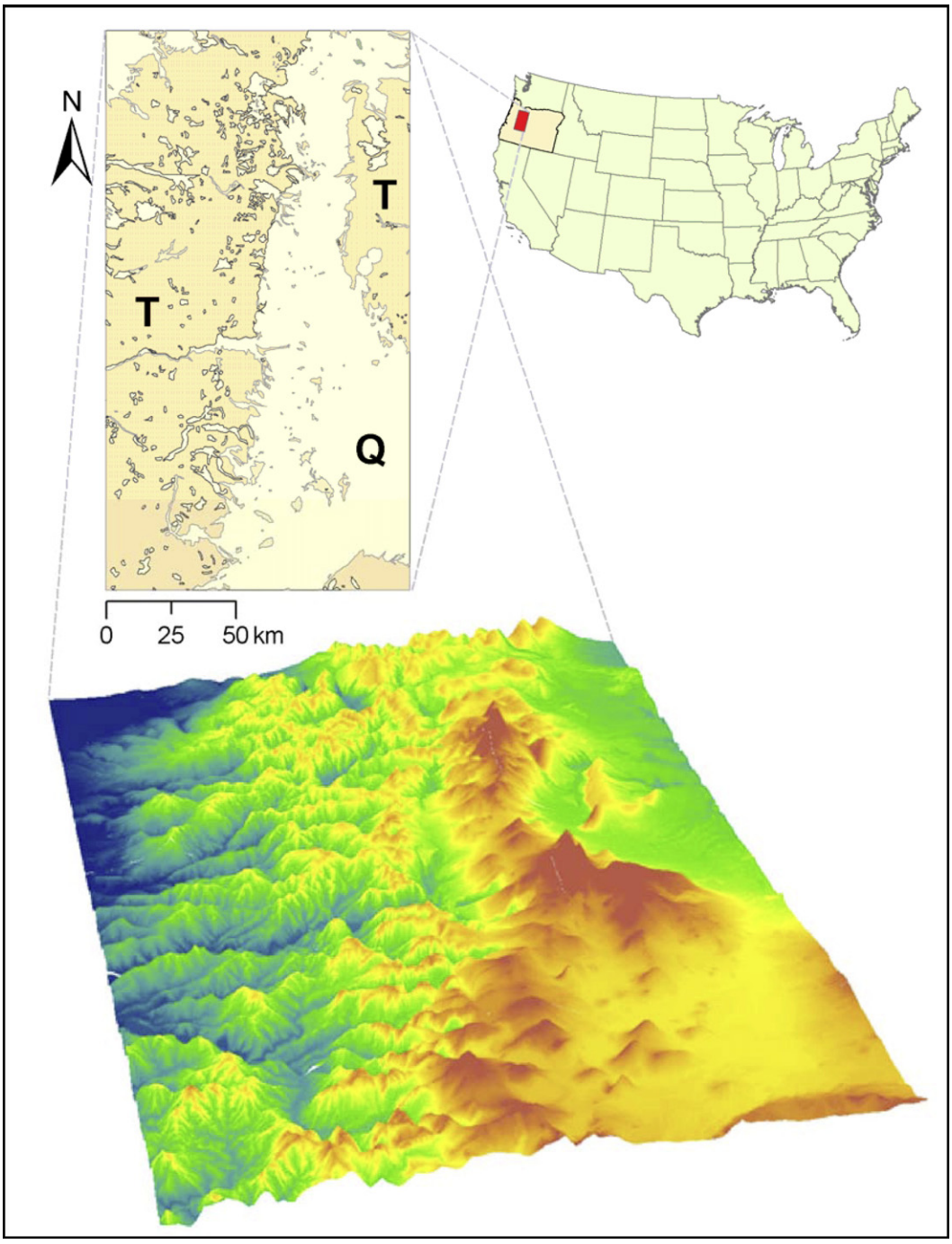

Fig. 1. Geographical, geological and topographic context of the study area. The upper insert shows a simplified geologic map with two age-based units: T = Tertiary, Q = Quaternary. The lower insert shows a perspective view illustrating the contrast in dissection between the western and eastern parts of the study area (blue-to-red color gradient corresponds to elevations ranging from 24 to 3200 m). The western part (Western Cascades) is characterized by low elevation and high local relief. The eastern part (High Cascades) is characterized by high elevation and low local relief.

1993). Denoting the elevation field by $z=f(x, y)$, κ_t is given by

$$\kappa_t = \frac{f_{xx}f_y^2 - 2f_{xx}f_xf_y + f_{yy}f_x^2}{\left(f_x^2+f_y^2\right)\sqrt{1+f_x^2+f_y^2}}, \quad (1)$$

where subscripts indicate differentiation. The positive values of κ_t indicate concave upward (U-like shape) morphology corresponding to valleys. In order to minimize the noise, the values of κ_t are calculated analytically for each cell in the raster using a polynomial approximation to the local patch of the surface defined on a 5×5 cells neighborhood centered on a focus cell. The valley segments are identified as regions with $\kappa_t>\kappa_0$, where κ_0 is a threshold above which a terrain is considered sufficiently upward curved to be a valley. The binary raster with cells corresponding to identified segments having a value of 1 and the remaining cells having a value of

0 is subjected to a series of image processing transformations (for details see Molloy and Stepinski, 2007) aimed at separating valleys from other landforms fulfilling the $\kappa_t > \kappa_0$ condition. These include masking designed to exclude segments having geometry irreconcilable with valleys, thinning to reduce valley segments to a single pixel thickness, and reconnecting to link the thinned channel segments into an integrated network.

Fig. 2 shows the results of automatic mapping of streams in our study area using different delineation algorithms. The shaded relief of the study area showing the dissection contrast between its western and eastern parts is given in panel (a). Panel (b) shows a "ground truth" map of the streams, the 1:100,000 scale "River Reach Shapefile" (http://www.gis.state.or.us/data/alphalist.html) which was originally developed by the United States Geologic Survey (USGS) from either aerial photographs or from cartographic source materials using manual and automated digitizing methods (http://eros.usgs.gov/guides/dlg.html). Hereafter we will refer to this map as the USGS river data. The USGS river data is known to have accuracy issues (e.g., Morisawa, 1957; Coates, 1958; Mark, 1983), but it constitutes a sufficient ground truth for our purpose, as we are only interested in dissection patterns on large spatial scale. Panel (c) shows streams delineated by our method. Streams delineated by morphology-based algorithm of Tarboton and Ames (2001) are shown on panel (d), and panels (e)–(h) show streams delineated by the hydrology-based algorithm using the different channelization criteria (1)–(4) outlined above. We use

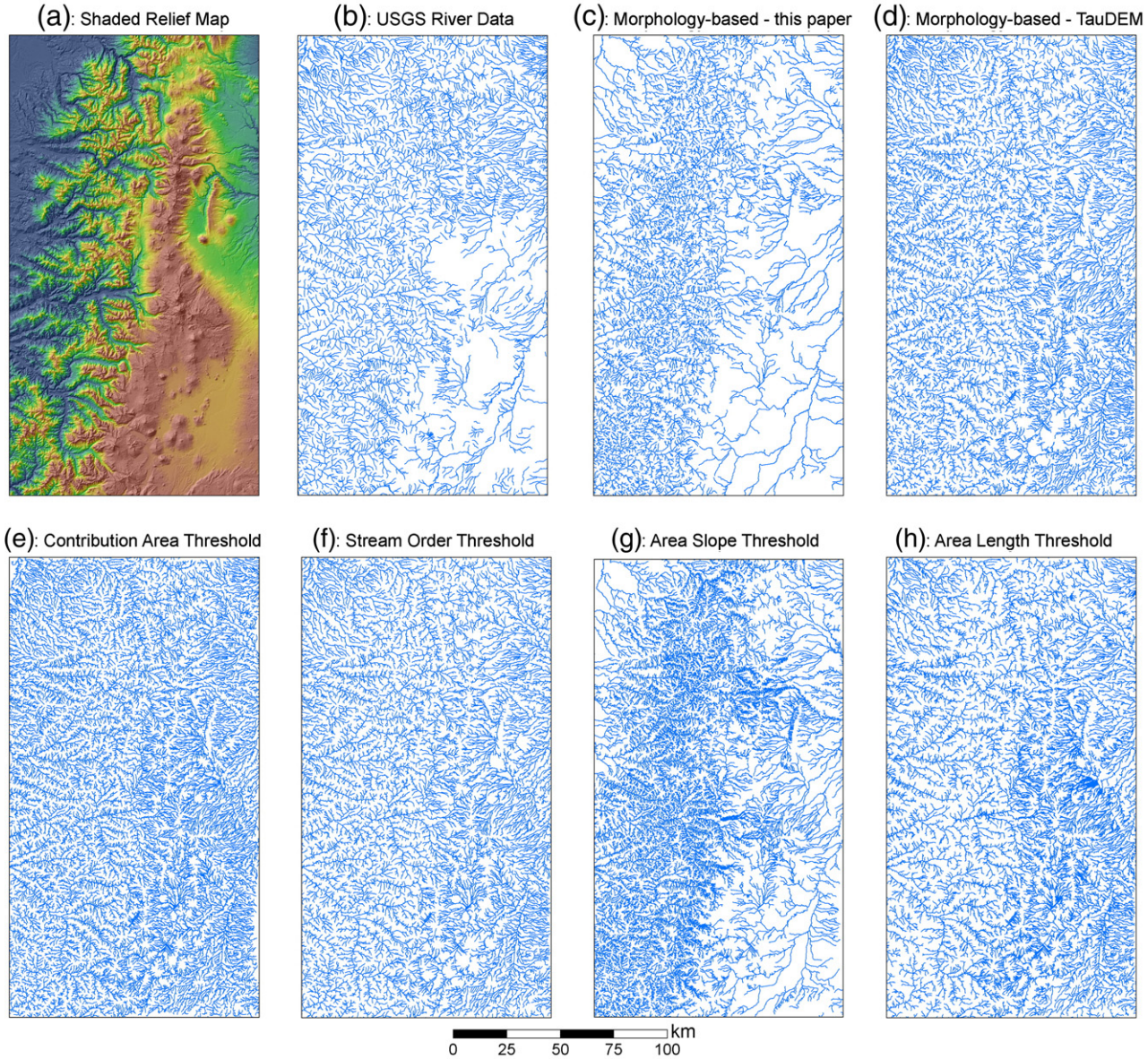

Fig. 2. Maps showing topography of the study area and results of stream delineation. (a) Shaded relief showing the dissection contrast. (b) USGS river data. (c) Streams delineated using the morphology-based algorithm of Molloy and Stepinski (2007). (d) Streams delineated using the morphology-based algorithm of Tarboton and Ames (2001) as implemented in TauDEM. (e)–(h) Streams delineated by the hydrology-based algorithm using different channelization criteria as indicated. See Table 1 for a summary of criteria and parameter values.

Table 1
The criteria, parameters and relative errors of algorithms used for extracting streams

Method/data set	Criterion and parameter values	Relative error of drainage density			
		Mean	Std. dev.	Min	Max
USGS "ground truth" rivers data	Independently derived from aerial photography and digitized by USGS.	0	0	0	0
This paper: morphology-based algorithm after Molloy and Stepinski (2007)	Curvature >0.003, flow accumulation >0	0.220	0.834	−0.964	9.729
Morphology-based algorithm of Tarboton and Ames (2001)	Curvature >0, flow accumulation >50	2.093	4.177	−0.711	57.266
Hydrology-based algorithm with contribution area threshold	Contribution area >300	2.966	4.995	−0.67	66.831
Hydrology-based algorithm with stream order threshold	Stream order >5	2.051	4.158	−0.727	54.415
Hydrology-based algorithm with contributing area and slope threshold	$AS^y > T$, $T=700$, $y=2.2$ (A is the $D\infty$ specific catchment area; S is the $D\infty$ slope)	1.237	1.813	−0.928	23.166
Hydrology-based algorithm with contributing area and stream length threshold	$A > M L^y$, $M=1.2$, $y=2.0$ (A is the $D8$ contributing area; L is the longest upstream flow path)	1.872	4.126	−0.743	51.64

TauDEM implementation of the last five delineation methods with threshold values chosen to get the density of dissection in the western part of the study area to be about the same as that of the USGS river data. The values of parameters used by all stream delineation algorithms are listed in Table 1.

Fig. 2 provides a visual comparison between the ground-truth dissection and dissection delineated by automatic algorithms. Only results from our algorithm (Fig. 2c) clearly reflect the spatial variation in dissection pattern between the western and eastern parts of the study area as seen in the USGS river map (Fig. 2b). The hydrology-based algorithms (Fig. 2e–h) are unable to map correctly the two different patterns of dissection. Only the map delineated using the slope contributing area threshold (Fig. 2g) offers a hint of the contrast because it provides higher dissection density for areas having higher local slope; however, even this map records the existing contrast much worse than our method. Perhaps the most surprising result is the poor performance of the morphology-based algorithm of Tarboton and Ames (2001) (Fig. 2d) that shows no contrast between the two parts of the study area. This is because their algorithm is sensitive to even the smallest positive curvature, and maps many features that are not proper valleys. The quantitative assessment of the different valley delineation algorithms, based on comparison of continuous drainage density, is given in Section 3.3.

3.2. Continuous drainage density map

Although our map of stream networks (Fig. 2c) most accurately identifies different densities and patterns of dissection in the two parts of the study area, the map of streams is a dataset designed for a visual inspection, and, as such, it is not well suited for a quantitative analysis necessary to determine factors controlling the dissection pattern. In order to perform such an analysis we transformed the map of streams into a continuous raster map of drainage density.

Drainage density, D, is a variable originally defined by Horton (1932) for an area unit as the total length of streams L_T in the unit divided by the total area of the unit A: $D=L_T/A$. So-defined D is an attribute of the area unit; it cannot describe changes in dissection density within the unit, and it does not constitute a good measure of spatial variability of dissection. Recently, Tucker et al. (2001) had introduced a variable $D(x, y)=1/(2<L(x, y)>)$ that is defined at any point in the landscape and can be interpreted as an at-point drainage density. Here $<L(x, y)>$ is the mean value of point-to-valley length $L(x, y)$, calculated over the neighborhood having a size equal to the autocorrelation length of $L(x, y)$ and centered at point (x, y). The autocorrelation length is the longest length lag over which the values of $L(x, y)$ are statistically related. $L(x, y)$ is the downslope distance to the nearest stream from a given point (x, y) following the path of steepest descent. This variable is defined for every cell in the raster and has a small value in places where stream network is dense and a large value in the places where the stream network is coarse. However, $L(x, y)$ is a random variable; two neighboring cells may have very different values of L because they may happen to be located at the two sides of the watershed boundary. Thus, L itself is not a suitable measure of dissection; instead we use $<L(x, y)>$ as a measure of dissection and half of its reciprocal as a measure of the drainage density (because a stream has tributaries from both sides). Note that $<L(x, y)>$ is locally-defined fundamental horizontal length scale associated with dissection. We compute $D(x, y)$ at every point in the raster to obtain a continuous map of drainage density.

3.3. Quantitative estimate of valley delineation accuracy

Fig. 3a shows the continuous drainage density map derived by applying the method of Tucker et al. (2001) to the DEM of our study area and using the streams as delineated by our morphology-based algorithm. An autocorrelation length of 3.7 km (or 100 cells) was used to calculate the average local downslope distance to the nearest stream. Comparison of Figs. 2c and 3a reveals how the two maps, streams and drainage density, show the same information from two different perspectives. We also calculated the continuous drainage density map based on the USGS river data, as well as the maps based on stream networks as delineated by hydrology-based algorithms and the morphology-based algorithm of Tarboton and Ames (2001). We use these maps to quantitatively assess the

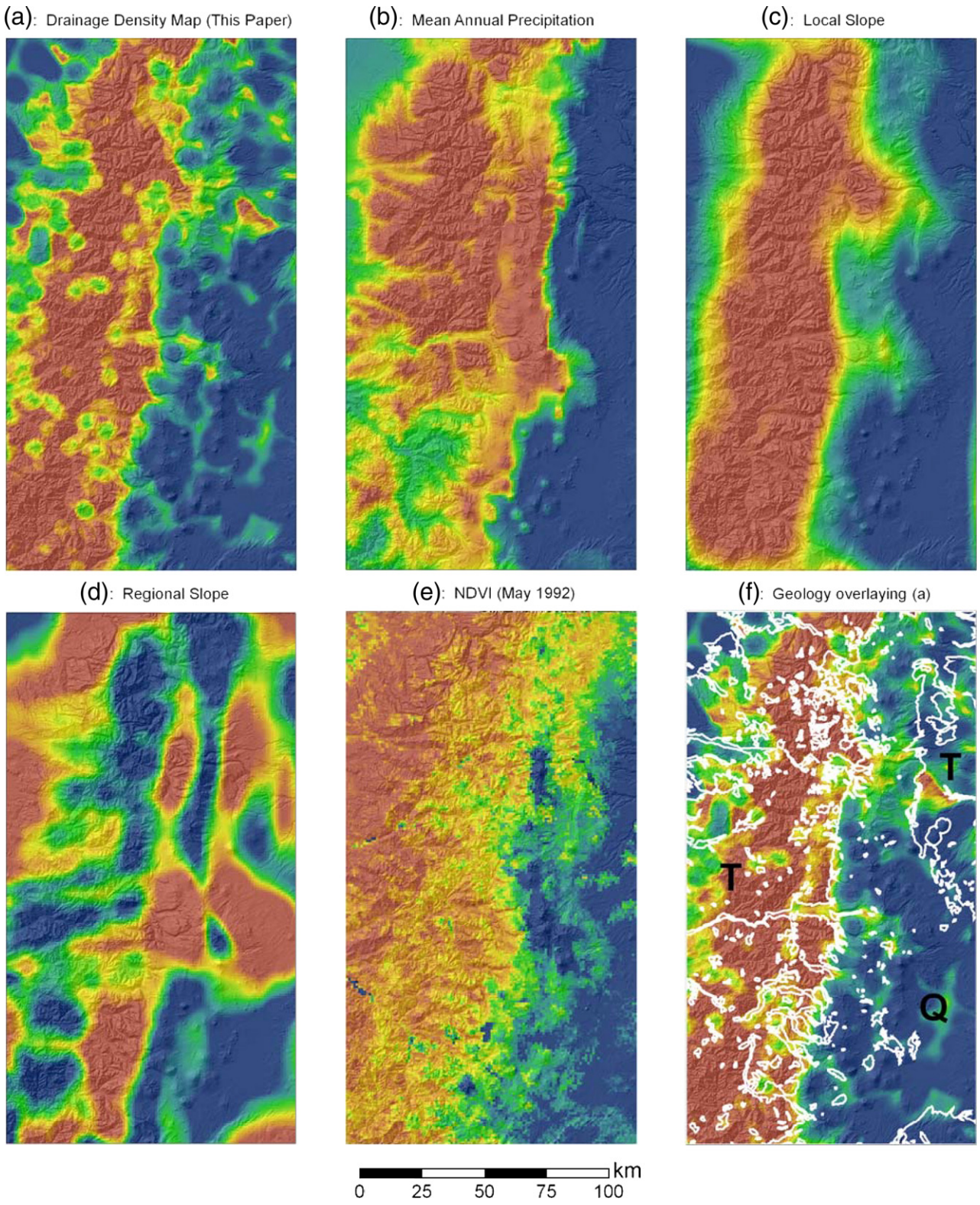

Fig. 3. Drainage density and environmental variables in the study area. (a) Continuous drainage density map based on streams extracted using morphology-based algorithm of Molloy and Stepinski (2007), min = 0.012 km^{-1}, max = 1.87 km^{-1}. (b) Mean annual precipitation, min = 245.45 mm, max = 3149.36 mm. (c) Local slope subject to low pass filter, min = 1.04°, max = 19.65°. (d) Regional slope at 31 km baseline, min = 0.002°, max = 2.623°. (e) Vegetation cover as given by the Normalized Difference Vegetation Index (NDVI, based on AVHRR data of May 1992), min = 0, max = 174. (f) Boundary of the simplified geologic map (shown as white lines) overlaying on top of the continuous drainage density map. The shaded relief is shown in the background for all maps.

performance of each algorithm by calculating statistics of relative difference between the drainage density derived from streams as delineated by a particular algorithm (D_m) and that derived from the USGS river data (D_t):

$$\Delta D = \frac{D_m - D_t}{D_t} \quad (2)$$

The values of ΔD are calculated at every cell in the raster and the statistical measures of these values (mean, standard deviation, minimum and maximum) are listed in Table 1. Our delineation algorithm yields drainage density map that has an order of magnitude smaller mean value of ΔD than maps yielded by the other algorithms. It is also characterized by a smallest value of standard deviation of ΔD. The distant second performer is the map derived from streams delineated by the hydrology-based algorithm using contributing area and slope thresholds (Fig. 2g). The worst performer is the map derived from streams delineated by the hydrology-based algorithm using contributing area threshold (Fig. 2e).

3.4. Controlling factors for spatial distribution of drainage density

Next, we use the map of drainage density to assess the roles of different environmental variables as control factors for drainage density. Plausible environmental variables that determine a regional pattern of drainage are: underlying geology and lithology (Wilson, 1971; Kelson and Wells, 1989), climate (Chorley, 1957; Gregory and Gardiner, 1975), vegetation (Melton, 1958), and topographic relief and slope (Schumm, 1956; Montgomery and Dietrich, 1989; Oguchi, 1997). The digital datasets containing measurements of these variables within our study area are available. We use mean annual precipitation as a measure of climate. The map of mean annual precipitation over the study area is acquired from the PRISM spatial climate dataset (PRISM Group, Oregon State University, http://www.prismclimate.org, created 4 Feb 2004) and shown in Fig. 3b. Maps of slopes are derived directly from the DEM. We consider slopes on two different scales: local slopes, calculated at the baseline equal to the raster cell, and the regional slope, calculated at the baseline of 31 km. The calculated raster of local slopes have been subjected to the low-pass filter in order to eliminate variations on small length scales; the resulting map is shown on Fig. 3c. The calculated map of regional slopes is shown on Fig. 3d. The spatial distribution of vegetation is approximated by the distribution of Normalized Difference Vegetation Index (NDVI), available in the North America Land Cover Characteristics Data Base (Brown et al., 1999) (http://edcsns17.cr.usgs.gov/glcc/). The map of NDVI is shown on Fig. 3e. Finally, as shown in Fig. 1, geology is extracted from the digital version of 1:500,000 scale Geologic Map of Oregon (Walker and MacLeod, 1991).

To assess the degree of control exerted by each environmental variable on the distribution of drainage density, we calculate the spatial correlation coefficient (Goodchild, 1986), ρ, between the map of D and the map of a variable. This coefficient measures the overall cross correlation between the two raster maps and is defined as:

$$\rho = \sum_1^n c_{ij} / \sqrt{\sum_1^n (z_i - \overline{z}_i)^2 \times \sum_1^n \left(z_j - \overline{z}_j\right)^2}, \quad (3)$$

where n is the total number of cells in the raster; i is any cell in the first grid; j is any cell in the second grid; z_i and z_j are the values of cells i and j, respectively; $\overline{z}_i$ and $\overline{z}_i$ are the mean values of the first and second grid, respectively; c_{ij} is a measure of similarity of cells i and j, $c_{ij}=(z_i-\overline{z}_i)\times(z_j-\overline{z}_j)$.

In our study area all environmental variables except for regional slope exhibit a dichotomy between the western and eastern parts (see Figs. 1, 2, and 3). The ultimate cause of this dichotomy is the different geology of the two parts as described in Section 2. We examine whether the sharp contrast in drainage density is directly due to geologic control, or rather due to other environmental variables mediating the influence of geology.

The correlation coefficient (ρ) between maps of D and precipitation is 0.55. However, the contrast line separating the high and low precipitation regions (Fig. 3b) does not coincide with the drainage density contrast (Fig. 3a) which is located farther west. This is because the west–east dichotomy in mean annual precipitation is due to the rain shadow effect and the precipitation contrast line separates the windward and leeward sites of the High Cascades. Therefore, despite a relatively high correlation between the maps of D and precipitation, the precipitation is not a major controlling factor responsible for the observed pattern of dissection. The map of local slope (Fig. 3c) is highly correlated with the map of D ($\rho=0.85$). However, high local slope is a corollary of dense dissection. Thus the high local slope is not a controlling factor of the drainage density, but rather a result of denser dissection. The map of regional slope (Fig. 3d) is poorly correlated with the map of D ($\rho=-0.093$), thus regional topography also does not control the pattern of dissection. The ρ coefficient between maps of D and vegetation (NDVI) is 0.46. The positive relationship between drainage density and vegetation is surprising because a negative relationship is expected (Melton, 1958) as vegetation cover enhances soil strength against runoff erosion and landsliding. Therefore, vegetation is not a controlling factor for drainage density; the observed correlation between the two maps is the result of interplay between climate, topography, and ultimately geology.

Unlike maps of precipitation and slopes, which are real-valued rasters, the simplified map of geology is a categorical raster. In order to calculate a correlation coefficient between drainage density and geology we have assigned numerical values of 1 to Q (Quaternary) and 2 to T (Tertiary), resulting in $\rho=0.57$. Thus, the correlation coefficient between the maps of geology and D is only slightly higher than that between the precipitation and D. Nevertheless, the major north–south boundary between the T and Q geological formations corresponds closely to the location where pattern of dissection changes sharply. This is illustrated in Fig. 3f where boundaries between the two formations are overlaid over the map of drainage density. The moderate value of a correlation coefficient

is explained by the presence of T unit in the far eastern portion of the study area where it is collocated with the relatively low drainage density. Thus, we conclude that geology is the dominant control factor for the spatial distribution of drainage density in the study area. This is further supported by calculating the zonal statistics of D within the zones of Q and T: the mean value of D in the Q zone (μ_Q=0.27, with standard deviation σ_Q=0.23 and number of sample n_Q=8,557,244) is significantly lower than that in the T zone (μ_T=0.71, with σ_T=0.37 and n_T=9437248), with $t=-2974.2 \gg t_{critical}=3.89$ at alpha level of 0.0001. Thus, the regional map of D primarily reveals the differences in the underlying geology. Other factors may contribute to spatial variations of drainage density, especially on smaller scales, but they do not control the overall pattern of dissection in the study area.

4. Discussion and conclusion

The map of continuous drainage density constructed for our study area reveals a sharp contrast in dissection pattern running roughly north-to-south and indicating abrupt change in some underlying factor (or factors) along the Q–T boundary line. We have analyzed correlations between the map of D and the maps of plausible controlling factors; we were able point to rock properties (referred to as geology) as the factor predominantly responsible for the observed contrast in D. The contrast in dissection pattern coincides with the main boundary between the Western and High Cascades and could be explained by different properties of rocks in the two units. The Western Cascades are older and the hydrothermal alteration of minerals (especially the formation of clays) tends to close pore spaces, reducing permeability and thus promoting surface runoff. This leads to more incision, steeper local slope, and higher drainage density (Ambers, 2001; Perron et al., 2004; Tague and Grant, 2004). The High Cascades are younger and much more permeable, thus promoting infiltration of water, reducing the surface runoff and resulting in less incision. Permeability data available for the study area (Ingebritsen et al., 1992, 1994) is based on measured groundwater flow and heat transport data, as well as computer modeling. For the youngest (0–2.3 Ma) rocks the permeability is estimated to be about 10^{-14} m^2, and for the oldest (18–25 Ma) rocks the permeability is estimated to be about 10^{-17} m^2. Thus, there is roughly three orders of magnitude difference in permeability between Q and T units.

The ability to infer geology, or at least some aspects of it, automatically from the topographic data provide affordable means of surveying large regions for which such information is not already available. Our results demonstrate a framework for inferring contrasts in geology, as well as other environmental spatial variables, from DEM data, which are readily available from remote sensing (e.g., Shuttle Radar Topography Mission data) for areas limited by physical access. The two technical aspects of our method, extraction of drainage networks and continuous mapping of drainage density have significance on their own. First, we have shown that automatic mapping of valleys on regional scale, where variations in dissection pattern are expected, cannot be achieved using the standard techniques build-in into popular software packages such as ESRI's ArcGIS and Rivix's RiverTools. Instead, a morphology-based delineation algorithm, such as that developed by Molloy and Stepinski (2007), needs to be used. Such algorithm offers a way to improve the accuracy of topographically derived datasets of streams, such as the USGS HYDRO1k that has a global coverage, but was constructed using channelization criteria based on contributing area and thus suffers from uniform drainage density leading to grossly inaccurate maps in parts of the world such as the Sahara desert, where pattern of dissection is highly variable. Second, we have demonstrated that the best way to quantitatively represent the dissection pattern is through a continuous map of drainage density. In our study area the dissection pattern reflects underlying geology, but, in some other regions it may also reflect other control factors such as climate. Sharp boundary in the map of D indicates spatial change in the dominant control factor; existence and location of such a contrast constitutes a discovery facilitated by our method. Follow up analysis is necessary to identify the actual nature of the dominant control factor.

In the case of our study area the controlling factors are known a priori. However, our method can be used to reveal and map the spatial variation of geology or other factors. This will be especially valuable for parts of the world that are not easy to access and/or with limited data available, such as the Sahara desert (Pena and Abdelsalam, 2006) or Northern Canada (Barnett et al., 2004). At the very least, the spatial variations revealed in the terrain dissection map derived from our method can be used as a guide or aid to help focus limited resource to interested areas. Our method also has great potential to reveal and explore underlying geology of other planets such as Mars.

Acknowledgements

We would like to acknowledge support by NASA (TFS under grant NNG05GM31G, WL under grant NNG04GJ71G). A portion of this research was conducted at the Lunar and Planetary Institute, which is operated by the USRA under contract CAN-NCC5-679 with NASA. This is LPI Contribution No. 1352. We thank Yi Qi for his help with initial data processing and Guido Ventura and an anonymous reviewer for their thorough and helpful reviews.

References

Ambers, R.K.R., 2001. Relationships between clay mineralogy, hydrothermal metamorphism, and topography in a Western Cascades watershed, Oregon, USA. Geomorphology 38, 47–61.

Band, L.E., 1986. Topographic partition of watersheds with digital elevation models. Water Resources Research 22, 15–24.

Barnett, P.J., Singhroy, V.H., Shirota, J., Leney, S.J., 2004. Methods for remote engineering geology terrain analysis in boreal forest regions of Ontario, Canada. Environmental & Engineering Geoscience 10, 229–241.

Bou Kheir, R., Chorowich, J., Abdallah, C., Dhont, D., 2007. Soil and bedrock distribution estimated from gully form and frequency: a GIS-based decision-tree model for Lebanon. Geomorphology 93, 482–492.

Brown, J.F., Loveland, T.R., Ohlen, D.O., Zhu, Z., 1999. The global land-cover characteristics database: the users' perspective. Engineering and Remote Sensing 65, 1069–1074.

Chorley, G., 1957. Climate and morphometry. Journal of Geology 65, 628–638.
Coates, D.R., 1958. Quantitative geomorphology of small drainage basins in southern Indiana. Technical Report 10, Office of Naval Research Project, Department of Geology, Columbia University, NR, 389-1042.
Costa-Cabral, M.C., Burges, S.J., 1994. Digital elevation model networks (DEMON): A model of flow over hillslopes for computation of contributing and dispersal areas. Water Resources Research 30, 1681–1692.
Goodchild, M.F., 1986. Spatial Autocorrelation. Catmog, vol. 47. Geo Books, Norwich.
Gregory, K.J., Gardiner, V., 1975. Drainage density and climate. Zeitschrift fur Geomorphologie 19, 287–298.
Horton, R.E., 1932. Drainage basin characteristics. American Geophysical Union Transactions 13, 348–352.
Howard, A.D., 1994. A detachment-limited model of drainage basin evolution. Water Resources Research 30, 2261–2285.
Ingebritsen, S.E., Sherrod, D.R., Mariner, R.H., 1992. Rates and patterns of groundwater flow in the Cascade Range volcanic arc, and the effect on subsurface temperatures. Journal of Geophysical Research 97 (B4), 4599–4627.
Ingebritsen, S.E., Mariner, R.H., Sherrod, D.R., 1994. Hydrothermal Systems of the Cascade Range, North-central Oregon. U. S. Geological Survey Professional Paper, vol. 1040-L. 86 pp.
Jenson, S.K., Domingue, J.O., 1988. Extracting topographic structure from digital elevation data for Geographic Information System analysis. Photogrammetric Engineering and Remote Sensing 54, 1593–1600.
Kelson, K.I., Wells, S.G., 1989. Geologic influences on fluvial hydrology and bedload transport in small mountainous watersheds, northern New Mexico, USA. Earth Surface Processes and Landforms 14, 671–690.
Kruse, F.A., Dietz, J.B., 1991. Integration of optical and microwave images for geologic mapping and resource exploration. Proceedings of the International Symposium on Remote Sensing of Environment, Thematic Conference on Remote Sensing for Exploration Geology. Environmental Research Institute of Michigan, Ann Arbor, pp. 535–548.
Lucieer, A., Orkhonselenge, T., Stein, A., 2004. Texture based segmentation for identification of geologic units in remotely sensed imagery. In: Franks, A., Grum, E. (Eds.), Proceedings of 3rd International Symposium on Spatial Data Quality. Technical University of Vienna, Austria, pp. 117–120.
Luo, W., Stepinski, T.F., 2006. Topographically derived maps of valley networks and drainage density in the Mare Tyrrhenum quadrangle on Mars. Geophysical Research Letters 33. doi:10.1029/2006GL027346.
Mark, D.M., 1983. Relations between field-surveyed channel networks and map-based geomorphometric measures, Inez, Kentucky. Annals of the Association of American Geographers 73, 358–372.
Melton, M.A., 1958. Correlation structure of morphometric properties of drainage systems and their controlling agents. Journal of Geology 66, 442–460.
Mitasova, K., Hofierka, J., 1993. Interpolation by regularized spline with tension: II. Application to terrain modeling and surface geometry analysis. Mathematical Geology 25, 657–669.
Molloy, I., Stepinski, T.F., 2007. Automatic mapping of valley networks on Mars. Computers and Geosciences 33, 728–738.
Montgomery, D.R., Dietrich, W.E., 1989. Source areas, drainage density, and channel initiation. Water Resources Research 25, 1907–1918.
Montgomery, D.R., Dietrich, W.E., 1992. Channel initiation and the problem of landscape scale. Science 255 (5046), 826–829.
Morisawa, M., 1957. Accuracy of determination of stream length from topographic maps. Transactions of the American Geophysical Union 38, 86–88.
O'Callaghan, J.F., Mark, D.M., 1984. The extraction of drainage networks from digital elevation data. Computer Vision, Graphics, and Image Processing 28, 323–344.
Oguchi, T., 1997. Drainage density and relative relief in humid steep mountains with frequent slope failure. Earth Surface Processes and Landforms 22, 107–120.
Peckham, S.D., 1995. Self-Similarity in the Three-Dimensional Geometry and Dynamics of Large River Basins. PhD Thesis, University of Colorado.
Pena, S.A., Abdelsalam, M.G., 2006. Orbital remote sensing for geological mapping in southern Tunisia: implication for oil and gas exploration. Journal of African Earth Sciences 44, 203–219.
Perron, J.T., Manga, M., Lamb, M.P., 2004. Permeability, Recharge, and Runoff Generation on Mars, Workshop on Martian Valley Networks. Smithsonian Institution, Washington D.C.
Peuker, T.K., Douglas, D.H., 1975. Detection of surface-specific points by local parallel processing of discrete terrain elevation data. Computer Graphics and Image Processing 4, 375–387.
Quinn, P., Beven, K., Chevallier, P., Planchon, O., 1991. The prediction of hillslope flow paths for distributed hydrological modelling using digital terrain models. Hydrological Processes 5, 59–80.
Schumm, S.A., 1956. Evolution of drainage systems and slopes in badlands at Perth Amboy, New Jersey. Geological Society of America Bulletin 67, 597–646.
Sherrod, D.R., Smith, J.G., 2000. Geologic Map of Upper Eocene to Holocene Volcanic and Related Rocks of the Cascade Range, Oregon, U.S. Geological Survey Geologic Investigations Series Map I-2569.
Tague, C., Grant, G.E., 2004. A geological framework for interpreting the low-flow regimes of Cascade streams, Willamette River basin, Oregon. Water Resources Research 40 (W04303). doi:10.1029/2003WR002629.
Tarboton, D.G., 1997. A new method for the determination of flow directions and upslope areas in grid digital elevation models. Water Resources Research 33, 309–320.
Tarboton, D.G., Ames, D.P., 2001. Advances in the Mapping of Flow Networks from Digital Elevation Data. World Water and Environmental Resources Congress. ASCE, Orlando, Florida.
Tucker, G.E., Catani, F., Rinaldo, A., Bras, R.L., 2001. Statistical analysis of drainage density from digital terrain data. Geomorphology 36, 187–202.
Van der Meer, F., 1998. Imaging spectrometry for geological remote sensing. Geologie en Mijnbouw 77, 137–151.
Walker, G.W., MacLeod, N.S., 1991. Geologic map of Oregon, special geologic map, 2 sheets. U.S. Geologic Survey, Reston, VA.
Wilson, L., 1971. Drainage density, length ratios, and lithology in a glaciated area of southern Connecticut. Geological Society of America Bulletin 82, 2955–2956.